Diffraction-free image transmission in kagome photonic lattices

2014 J. Opt. 16 015706

(http://iopscience.iop.org/2040-8986/16/1/015706)

IOP Publishing Journal of Optics
J. Opt. **16** (2014) 015706 (6pp) doi:10.1088/2040-8978/16/1/015706

Diffraction-free image transmission in kagome photonic lattices

Rodrigo A Vicencio and Cristian Mejía-Cortés

Departamento de Física, MSI-Nucleus on Advanced Optics, and Center for Optics and Photonics (CEFOP), Facultad de Ciencias, Universidad de Chile, Santiago, Chile

E-mail: rodrigov@uchile.cl

Received 14 September 2013, accepted for publication 7 November 2013
Published 28 November 2013

Abstract

We study the propagation of non-diffracting images in kagome photonic lattices. In a weak-coupling regime (discrete approach), the linear spectrum is composed by only three bands, including a completely degenerated and flat one. The states forming this special band are well localized in space and constitute *building blocks* for this lattice. By linearly combining these non-diffractive fundamental modes, different shapes can be composed and, therefore, a given image will propagate without distortion. As an example, we compare the linear propagation of a particular image for kagome and rectangular lattices. At the end, we test our concept by performing numerical simulations in a continuous kagome potential.

Keywords: waveguide arrays, diffraction-free propagation, image transmission, flat band systems

PACS numbers: 42.82.Et, 78.67.Pt, 42.30.-d

(Some figures may appear in colour only in the online journal)

1. Introduction

The propagation of diffraction-free beams has been an important subject of research in physics. A solution for this problem was suggested in 1987 [1] by using the concept of Bessel beams. These solutions are formed by coherently combining several plane waves possessing the same longitudinal propagation constants. On the other hand, photonic lattices have emerged as key setups to study fundamental aspects of linear and nonlinear wave dynamics of periodic and aperiodic systems. Nowadays, diverse topologies and geometries are fabricated or induced by very controlled and accessible techniques [2, 3]. *Diffraction-free image transmission* is an important area of research where the fundamental properties of waveguide arrays can be used for concrete applications. The connection between image transmission and waveguide arrays was explored in [4] by studying the propagation of extended non-diffracting beams in a two-dimensional (2D) square photonic lattice. For example, in [5] the authors proposed, theoretically and experimentally, waveguide arrays with a segmentation in the propagation coordinate allowing robust image reconstruction. Diffraction-free transmission of complex light patterns has been proposed, and experimentally observed, by implementing a modulation of the refractive index along the waveguides in laser-written [6] as well as photo-induced [7] photonic lattices. Reference [8] explores the propagation of complex stable solitons in 2D lattices, as nonlinear transmission of images of arbitrary shape. Very recently, image transmission has been studied by using the properties of disordered one-dimensional lattices applying the concept of self-imaging by segmentation [9]. In addition, high-fidelity quantum transport has been observed in photonic lattices [10], by designing a very specific coupling dependence.

Kagome lattices (see figure 1) have been historically studied as a model for geometrically frustrated magnetism [11] and for presenting flat bands [12]. These lattices have been implemented only very recently in different contexts of physics like electronics [13], ultracold atoms [14] and/or plasmonic [15]. In the context of photonic lattices, a refraction index pattern with a kagome geometry was already implemented in optically induced lattices [16], and could be implemented as well in femtosecond laser-writing waveguide arrays [17].

Flat band systems possess at least one band that is completely flat or thin compared to the next energy gap. Light propagating in such a system will experience zero or very low diffraction, as a consequence of an abrupt

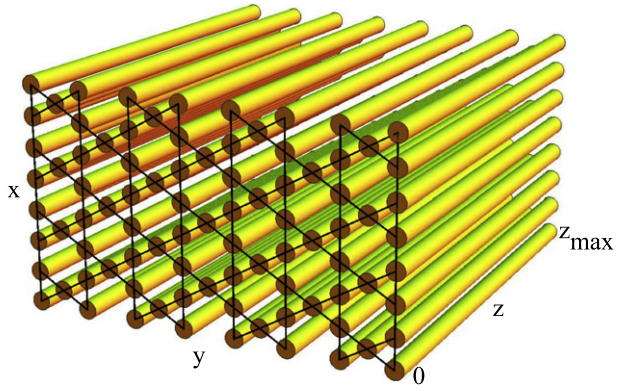

Figure 1. A kagome photonic lattice composed by a set of ordered optical waveguides. Nearest-neighbor interactions are represented by lines connecting waveguides.

reduction of the dispersion coefficient. The idea of having a flat region in the linear spectrum, to cancel the diffraction of beams and/or images, was numerically suggested in [18, 19], and experimentally observed in [20], for specially designed photonic crystals. More recently, a non-diffractive regime was suggested for photonic crystals presenting a modulation in the propagation direction [21], including the observation of two-dimensional image transmission.

In this paper, we propose a novel scheme for transmitting non-diffracting images by using the particular properties of a kagome photonic lattice. The band structure of this lattice includes a flat band with zero diffraction. The localized modes belonging to this band can be linearly combined to form different images and a perfect transmission of any constructed pattern is observed for arbitrary long propagation distances. We compare our findings with typical rectangular lattices to emphasize the particular properties of kagome systems. At the end, we corroborate our results with continuous numerical simulations considering a kagome optical potential.

2. Discrete model and linear spectrum

In the coupled-mode approximation (discrete approach), the evolution of the field amplitude along a normalized propagation direction z, in a defined lattice, is described by a discrete Schrödinger equation [2, 3]:

$$-\mathrm{i}\frac{\partial u_{\vec{n}}}{\partial z} = \sum_{\vec{m}} V_{\vec{n},\vec{m}} u_{\vec{m}}, \tag{1}$$

where $u_{\vec{n}}$ represents the field amplitude at site $\vec{n}$ of a 2D kagome lattice. The coupling function $\sum_{\vec{m}} V_{\vec{n},\vec{m}} u_{\vec{m}}$ defines the lattice structure by describing the linear interactions between $u_{\vec{n}}$ and its nearest neighbors (represented by lines in figure 1). The optical power, defined as $P \equiv \sum_{\vec{n}} |u_{\vec{n}}|^2$, is a conserved quantity of model (1). We use the participation ratio

$$R \equiv P^2 \Big/ \sum_{\vec{n}} |u_{\vec{n}}|^4, \tag{2}$$

to characterize the effective size of the wavepacket. R is an indicator of how many lattice sites are effectively excited in a particular array. For an excitation having M equal amplitudes and a zero background (surrounding sites), $R = M$.

Linear solutions are obtained by solving model (1) with a stationary ansatz of the form $u_{\vec{n}}(z) = u_{\vec{n}} \exp(\mathrm{i}\lambda z)$. The parameter λ defines the longitudinal propagation constant or spatial frequency. We obtain the linear spectrum by considering the unit cell of the lattice, corresponding to any triangle of three sites in figure 1. We construct the corresponding 2D $\vec{k}$ vectors by considering a lattice constant equal to 1 between nearest-neighbor sites, obtaining the following dispersion relation [12]:

$$\lambda(k_x, k_y) = -2, \qquad 1 \pm \sqrt{1 + 8f(k_x, k_y)}, \tag{3}$$

where $f(k_x, k_y) \equiv 1 + \cos^2(k_x/2)[2\cos^2(k_x/2) - 3] + \cos^2(\sqrt{3}k_y/2)[2\cos^2(k_x/2) - 1]$. Figure 2(a) shows a 3D plot of the band structure in the first Brillouin zone. The upper and lower bands are connected at $\lambda = 1$ by six Dirac points located at the vertices of the Brillouin zone. The third band corresponds to a completely degenerated and flat band, located exactly at $\lambda = -2$ (this band coincides with the region defined as the first Brillouin zone in figure 2(a) corresponding to a hexagon with vertices defined as $f(k_x, k_y) = -1/8$).

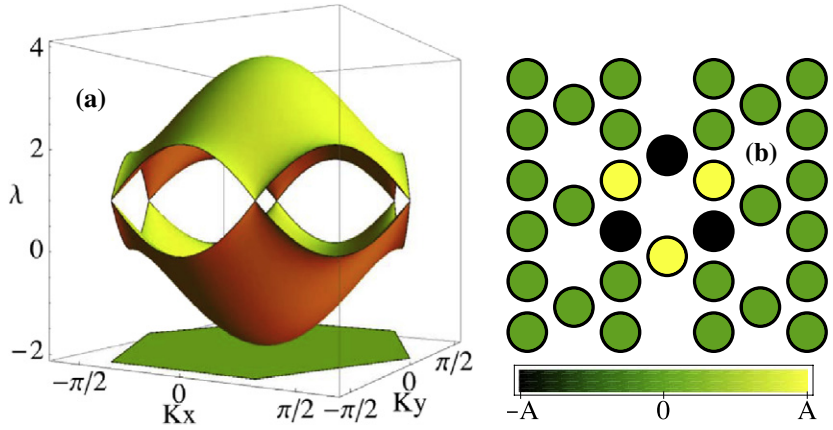

Figure 2. (a) Band structure of a kagome lattice in the first Brillouin zone. (b) Example of a ring mode of amplitude A belonging to the flat band $\lambda = -2$.

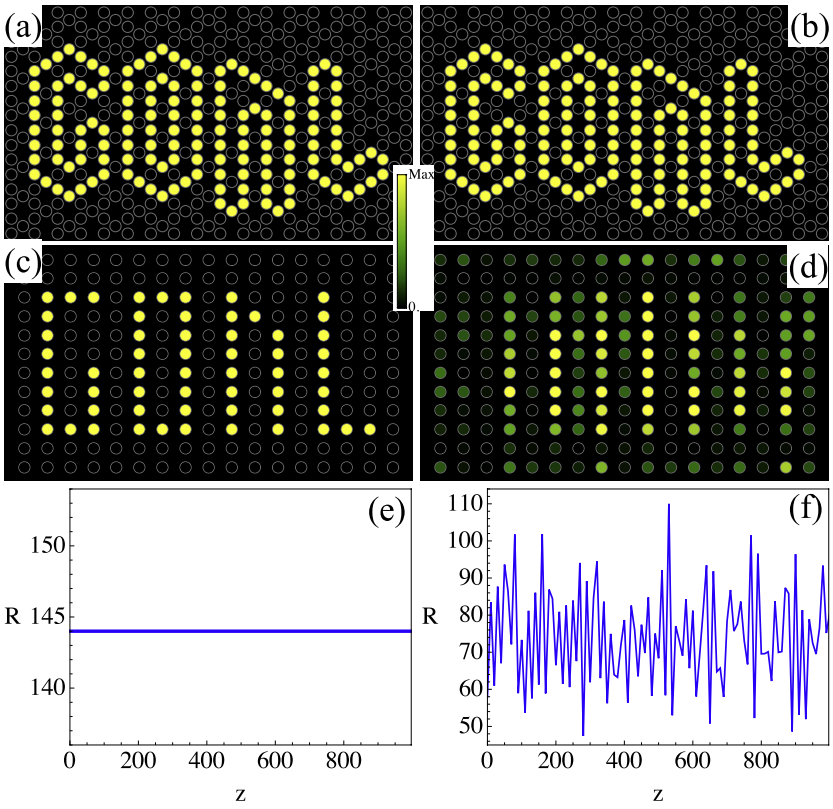

Figure 3. (a) Input $|u_{\vec{n}}(0)|^2$ and (b) output $|u_{\vec{n}}(z_{\max})|^2$ power profiles for a kagome lattice. (c) Input and (d) output power profiles for a square lattice. (e) and (f) R versus z for a kagome and a square lattice, respectively.

This flat band is formed with as many states as the number of closed six-site rings in the lattice. These states are called 'ring' modes [22] and possess six peaks with equal amplitude but alternating phase (sign), with a strictly zero background (see figure 2(b)). These linear modes are independent of the system size, being very well localized in the lattice ($R = 6$). In general, all linear modes of any homogeneous periodic lattice are completely extended [2, 3]. However, a particular feature of a flat band system is the possibility to construct very localized eigenmodes as a destructive linear combination of extended linear wavefunctions [12]. In the kagome case, the flat band possesses extended staggered loop states. Ring modes are formed by linearly combining these loop states, preserving their frequency and generating a very localized profile.

3. Image transmission

These modes constitute '*building blocks*' in our image propagation scheme and we will write them as $K^{\mathrm{c}}_{\vec{n}}$, where c defines the center position of the ring mode. Any linear combination of them will form an exact linear stationary solution of the system that will propagate without diffraction for any given distance:

$$u_{\vec{n}}(0) = \sum_{c} K^{\mathrm{c}}_{\vec{n}} \rightarrow |u_{\vec{n}}(z)|^2$$

$$= \left| \sum_{c} K^{\mathrm{c}}_{\vec{n}} \exp(-2\mathrm{i}z) \right|^2 = |u_{\vec{n}}(0)|^2,$$

i.e., a constant pattern (image). All the ring modes belonging to this special flat band possess a zero group velocity and zero diffraction coefficient. This guarantees that the images will propagate along the propagation direction without destroying and will be completely immobile across the lattice.

We take advantage of this property and focus on the propagation of an image formed as a combination of several ring modes. Any wished symbol or image will propagate stably along the propagation coordinate because they generate a perfectly coherent linear combination. For example, we construct the word '*GONL*' as an initial condition (see figure 3(a)) by linearly combining 35 ring modes. The profile has 144 amplitudes of alternating signs, with zero amplitude sites in the superposition region. We propagate this image along the lattice up to, in this example, $z_{\max} = 1000$. In figure 3(b) the output profile shows, as predicted, a diffraction-free image transmission without any distortion. By inspecting the evolution of the participation ratio (figure 3(e)), we observe that there is no single change in the profile, with a constant value of $R = 144$ along z. In principle, the propagation of any shape is possible, but considering the special topology of the lattice and the possible ways to combine building blocks. As soon as our lattice possesses one closed ring, a ring mode will be a stationary solution of the system with $\lambda = -2$. Therefore, the possibilities of transmitting composed images will depend on the number of closed rings present in the lattice with no size effects affecting our scheme.

For comparison purposes, we propagate the same word (but different structure) in a homogeneous rectangular lattice (see figure 3(c)), which is a common framework in different contexts of physics [2, 3]. This type of lattice has no degenerated band and no localized building block mode. All the linear modes belong to a unique band and are completely extended ($\sim \sin k_x n \cdot \sin k_y m$). The only possible pattern to be observed during propagation, independent of the word and its structure, corresponds to a combination of discrete diffraction patterns [23], as shown in figure 3(d). If we take a look at the evolution of R in figure 3(f), we observe a complete destruction of the initial image. Different spatial frequencies are excited in the dynamics (non-coherent profile), resulting in a strong diffraction and distortion for square lattices. Therefore, no well defined (localized) diffraction-free images can be propagated in this type of lattice.

3.1. Image transmission: continuous approach

Our previous results, based on the discrete model (1), assumed an array of weakly interacting waveguides. From an experimental point of view, that approach matches perfectly to the experiments developed in fabricated lattices [17], where the effective coupling between waveguides is weak and second-order interactions are negligible. However, when thinking on induced lattices [16], presenting a continuous periodic potential, this approach is not valid anymore. Therefore, in order to study how robust our results on image transmission are, we study the propagation of ring modes and images by using a continuous approach. We consider a Schrödinger-type paraxial wave equation, including a transversal periodic modulation of the normalized refractive index, given by [4]

$$i\frac{\partial \psi}{\partial z} + \frac{1}{2}\nabla_\perp^2 \psi + V(x,y)\psi = 0, \tag{4}$$

where $\psi(x, y, z)$ corresponds to the slowly varying amplitude of the optical field and $\nabla_\perp^2 \equiv \partial_x^2 + \partial_y^2$ is the transversal Laplacian operator. $V(x, y) \equiv V_0 f(x, y)$ defines the optical potential, V_0 being the lattice depth (proportional to the refractive index contrast) and

$$f(x,y) = \left[\cos(y) - \cos\left(\sqrt{3}x/2\right)\cos(y/2)\right]^2 + 3\sin^2\left(\sqrt{3}x/2\right)\sin^2(y/2),$$

a kagome lattice structure [16]. The discrete approximation (1) is recovered for deep potential wells (large V_0), where the tunneling between lattice sites is weaker and only nearest-neighbor interactions are relevant. The periodic potential $V(x, y)$ implies a complete band structure and not only three bands as in the discrete approximation (1). Therefore, it becomes important to study how robust the ring modes and their combinations are, and the persistence of the flat band phenomenology. To characterize solutions, we compute R by replacing sums by integrals in expression (2) as a measure of the size of a particular profile. To facilitate our analysis, we normalize this value to the value of a Gaussian excitation in a single potential well (R_g), defining $\bar{R} \equiv R/R_g$ as an indicator of how many lattice 'sites' are effectively excited.

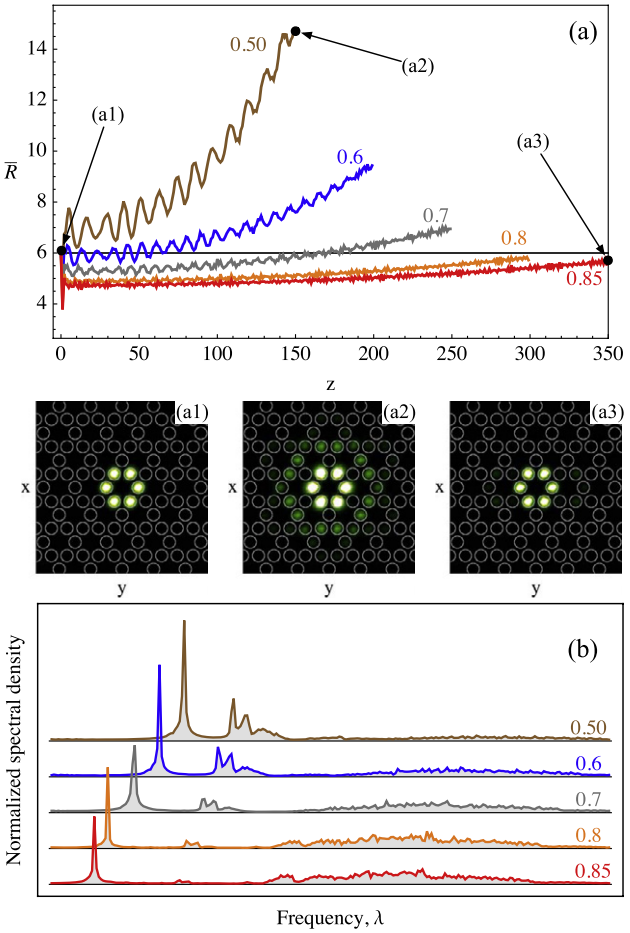

Figure 4. (a) $\bar{R}$ versus z for a 'ring' input condition (horizontal black line indicates $\bar{R}(0)$). Insets (a1)–(a3) show output power spatial profiles for the parameters indicated in (a). (b) Normalized frequency spectrum. V_0 is indicated in the figures.

We solve model (4) by using a beam propagation method (BPM) based on the fast-Fourier transform split-step numerical algorithm. The second-order derivative terms in x and y are solved analytically in Fourier space. Consequently, we apply periodic boundary conditions in x and y. The linear term in the equation was solved, in real space, by using a fourth-order Runge–Kutta method. In order to study the possibility to propagate ring mode profiles in a continuous context, we defined a normalized propagation distance z_{max}, which depends on the lattice depth. For a given value of V_0, z_{max} is defined as the longitudinal distance for which a single Gaussian excitation ($\bar{R} = 1$), initially centered in a potential well, diffracts across the whole system ($\bar{R} \sim 70$). To mimic a discrete ring mode, such as the one shown in figure 2(b), we construct an initial profile by superposing six Gaussian beams ($\bar{R} = 6$), with alternating phases, distributed at the first potential wells around the center of the lattice (see figure 4(a1)). Thus, the initial condition is written as

$$\psi(\vec{r}, z=0) = \psi_0 \sum_{l=1}^{6} e^{-0.5|\vec{r}-\vec{n}_l|^2} e^{i\pi l}, \tag{5}$$

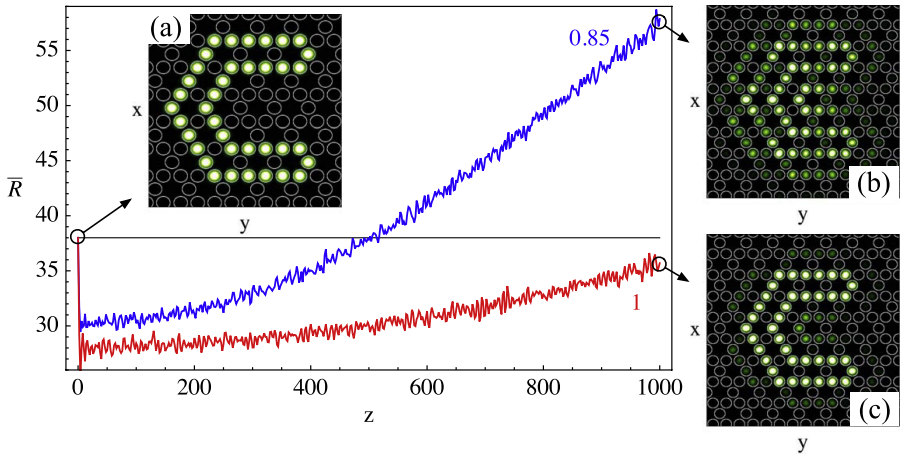

Figure 5. $\bar{R}$ versus z for a 'C' input condition for V_0 indicated in the figure. Insets show power spatial profiles at (a) $z = 0$ and (b)–(c) $z = 1000$.

where ψ_0 is the amplitude of each Gaussian beam and $\vec{r}_l$ corresponds to a transversal lattice position for which $V(\vec{r}_l)$ is a minimum. We explore different V_0 values and study the evolution of the normalized participation ratio as a measure of the stability and robustness of the propagating profile. In figure 4(a) we show our results for the initial configuration shown in figure 4(a1). For shallow lattices, we observe that the ring profile tends to diffract, increasing its participation ratio faster (as an example, see figure 4(a2)). Nevertheless, we observe that the ring profile is strongly preserved accompanied by the excitation of other linear modes. However, once the potential is strong enough, the light is better trapped in each potential well (see figure 4(a3)), observing an almost perfect propagation of the ring mode. In general, we observe a stable propagation of ring mode profiles for all tested V_0, but enhanced for deeper lattices. To complement our analysis, we computed a longitudinal frequency spectrum by implementing a Fourier transform along the propagation coordinate [24]. This analysis gives us the longitudinal excited frequencies as a direct manifestation of the band structure. In figure 4(b) we show the frequency spectrum for different V_0 values. We identify a well defined single peak as evidence of the excitation of a flat band. We see how this peak becomes thinner, and the following right-side gap wider, for an increasing value of V_0, fulfilling the flat band definition requirements. Therefore, even though the flat band has a nonzero width in a continuous model, their states have an almost equal propagation constant and small transversal velocities (weak dispersion). This is a necessary ingredient for approaching the diffraction-free image regime predicted for a discrete model. For all tested values, the flat band was effectively excited with the initial condition (5), which is indeed a non-stationary mode of model (4).

Finally, we prove the concept of image transmission explored in figure 3 by combining several ring modes (5) and studying their propagation (see figure 5). As an example, we explore the propagation of a letter 'C', formed by linearly combining 9 ring profiles (see figure 5(a)) for two deep optical potentials. We observe how the participation ratio initially decreases due to mode adjustments in each potential well. Then, $\bar{R}$ starts to increase due to the excitation of different linear propagating modes, belonging to different bands of the system. For $V_0 = 0.85$, the image tends to destabilize faster, keeping only some features of the initial letter (see figure 5(b)). By increasing the potential depth to $V_0 = 1$, we observe a stable propagation of the letter with a very slow increment of the normalized participation ratio. For $z_{max} = 1000$, we observe that the initial image continues propagating very stably (see figure 5(c)), with only small linear waves in the surroundings. In order to propagate a more complex image/pattern (composed by several ring profiles), we will require to consider a larger system, to avoid reflection at borders that could affect the image stability and deeper potential wells to guarantee a stable propagation.

Finally, when considering nonlinearity, for example a Kerr-like medium, we observe two very different regimes. For a focusing nonlinearity, the effective frequency of the profile shifts from $\lambda = -2$ to larger values, therefore crossing the linear bands and interacting with the modes belonging to them, which finally produces an increment of the effective size of the wavepacket [24]. On the other hand, when the nonlinearity is negative the effective frequency of the profile decreases and enters into the gap, tending to localize the light and, therefore, decreasing the effective size of the profile. However, nonlinear ring modes are stable only for very low levels of power [22], so therefore a combination of multiple rings must promote the destruction of the image for larger powers (increasing nonlinear effect).

4. Conclusions

In conclusion, we have shown that a linear kagome lattice allows transmission of non-diffracting images. The key ingredient is the understanding of the localized ring modes belonging to the flat band (truly flat in a discrete model and thin in a continuous one) of this lattice. Any linear combination of these modes will form a given image that can be transmitted along the waveguide array. Our results show that our prediction based on a discrete model can

be extrapolated to deep continuous lattices. Our concept could have a strong impact in linear transmission schemes, suggesting the propagation of arbitrary images for very low levels of power, which is certainly a very important issue for all-optical applications. It is worth mentioning that these ideas could also find a direct application in hollow fiber transmission systems [25]. Finally, similar properties could be explored in wire metamaterials [26], increasing the diversity of possible applications.

Acknowledgments

Authors thank A Szameit, Y S Kivshar and M I Molina for useful discussions. We acknowledge funding from FONDECYT Grants 1110142, Programa ICM P10-030-F and Programa de Financiamiento Basal de CONICYT (FB0824/2008).

References

[1] Durnin J 1987 Exact solutions for nondiffracting beams. I. The scalar theory *J. Opt. Soc. Am.* A **4** 651
Durnin J, Miceli J J and Eberly J H 1987 Diffraction-free beams *Phys. Rev. Lett.* **58** 1499
[2] Lederer F, Stegeman G I, Christodoulides D N, Assanto G, Segev M and Silberberg Y 2008 Discrete solitons in optics *Phys. Rep.* **463** 1
[3] Chen Z, Segev M and Christodoulides D N 2012 Optical spatial solitons: historical overview and recent advances *Rep. Prog. Phys.* **75** 086401
[4] Manela O, Segev M and Christodoulides D N 2005 Nondiffracting beams in periodic media *Opt. Lett.* **30** 2611
[5] Longhi S 2008 Image reconstruction in segmented waveguide arrays *Opt. Lett.* **33** 473
Szameit A, Dreisow F, Heinrich M, Pertsch T, Nolte S, Tünnermann A, Suran E, Louradour F, Barthélémy A and Longhi S 2008 Image reconstruction in segmented femtosecond laser-written waveguide arrays *Appl. Phys. Lett.* **93** 181109
[6] Kartashov Y V, Szameit A, Vysloukh V A and Torner L 2009 Light tunneling inhibition and anisotropic diffraction engineering in two-dimensional waveguide arrays *Opt. Lett.* **34** 2906
Szameit A, Kartashov Y V, Dreisow F, Heinrich M, Pertsch T, Nolte S, Tünnermann A, Vysloukh V A, Lederer F and Torner L 2009 Inhibition of light tunneling in waveguide arrays *Phys. Rev. Lett.* **102** 153901
[7] Zhang P, Efremidis N K, Miller A, Hu Y and Chen Z 2010 Observation of coherent destruction of tunneling and unusual beam dynamics due to negative coupling in three-dimensional photonic lattices *Opt. Lett.* **35** 3252
[8] Yang J, Zhang P, Yoshihara M, Hu Y and Chen Z 2011 Image transmission using stable solitons of arbitrary shapes in photonic lattices *Opt. Lett.* **36** 772
[9] Keil R, Lahini Y, Shechtman Y, Heinrich M, Pugatch R, Dreisow F, Tünnermann A, Nolte S and Szameit A 2012 Perfect imaging through a disordered waveguide lattice *Opt. Lett.* **37** 809
Heinrich M, Keil R, Lahini Y, Naether U, Dreisow F, Tünnermann A, Nolte S and Szameit A 2012 Disorder-enhanced nonlinear delocalization in segmented waveguide arrays *New J. Phys.* **14** 073026
[10] Perez-Lejía A, Keil R, Kay A, Moya-Cessa H, Nolte S, Kwek L C, Rodríguez-Lara B M, Szameit A and Christodoulides D N 2013 Coherent quantum transport in photonic lattices *Phys. Rev.* A **87** 012309
[11] Atwood J L 2002 Kagome lattice: a molecular toolkit for magnetism *Nature Mater.* **1** 91
[12] Bergman D L, Wu C and Balents L 2008 Band touching from real-space topology in frustrated hopping models *Phys. Rev.* B **78** 125104
[13] Wang L, Terhalle B, Guzenko V A, Farhan A, Hojeij M and Ekinci Y 2012 Generation of high-resolution kagome lattice structures using extreme ultraviolet interference lithography *Appl. Phys. Lett.* **101** 093104
[14] Jo G B, Guzman J, Thomas C K, Hosur P, Vishwanath A and Stamper-Kurn D M 2012 Ultracold atoms in a tunable optical kagome lattice *Phys. Rev. Lett.* **108** 045305
[15] Nakata Y, Okada T, Nakanishi T and Kitano M 2012 Observation of flat band for terahertz spoof plasmons in a metallic kagome lattice *Phys. Rev.* B **85** 205128
[16] Boguslawski M, Rose P and Denz C 2011 Nondiffracting kagome lattice *Appl. Phys. Lett.* **98** 061111
[17] Szameit A, Burghoff J, Pertsch T, Nolte S, Tuennermann A and Lederer F 2006 Two-dimensional soliton in cubic fs laser written waveguide arrays in fused silica *Opt. Express* **14** 6055
[18] Kosaka H, Kawashima T, Tomita A, Notomi M, Tamamura T, Sato T and Kawakami S 1999 Self-collimating phenomena in photonic crystals *Appl. Phys. Lett.* **74** 1212
[19] Chigrin D N, Enoch S, Sotomayor Torres C M and Tayeb G 2003 Self-guiding in two-dimensional photonic crystals *Opt. Express* **11** 1203
[20] Iliew R, Etrich C, Peschel U, Lederer F, Augustin M, Fuchs H-J, Schelle D, Kley E-B, Nolte S and Tünnermann A 2004 Diffractionless propagation of light in a low-index photonic-crystal film *Appl. Phys. Lett.* **85** 5854
[21] Staliunas K and Herrero R 2006 Nondiffractive propagation of light in photonic crystals *Phys. Rev.* E **73** 016601
[22] Vicencio R A and Johansson M 2013 Discrete flat-band solitons in the kagome lattice *Phys. Rev.* A **87** 061803(R)
[23] Szameit A, Pertsch T, Dreisow F, Nolte S, Tünnermann A, Peschel U and Lederer F 2007 Light evolution in arbitrary two-dimensional waveguide arrays *Phys. Rev.* A **75** 053814
[24] Naether U, Martínez A J, Guzmán-Silva D, Molina M I and Vicencio R A 2013 Self-trapping transition in nonlinear cubic lattices *Phys. Rev.* E **87** 062914
Naether U, Heinrich M, Lahini Y, Nolte S, Vicencio R A, Molina M I and Szameit A 2013 Self-trapping threshold in disordered nonlinear photonic lattices *Opt. Lett.* **38** 1518
[25] Argyros A and Pla J 2007 Hollow-core polymer fibres with a kagome lattice: potential for transmission in the infrared *Opt. Express* **15** 7713
Wang Y Y, Wheeler N V, Couny F, Roberts P J and Benabid F 2011 Low loss broadband transmission in hypocycloid-core kagome hollow-core photonic crystal fiber *Opt. Lett.* **36** 669
[26] Simovski C R, Belov P A, Atrashchenko A V and Kivshar Y S 2012 Wire metamaterials: physics and applications *Adv. Mater.* **24** 4229